AD-A254 403

NTATION PAGE

Form Approved
OBM No. 07[illegible]0188

Date. 1992	3. Report Type and Dates Covered. Final - Proceedings

4. Title and Subtitle.
The Classical Scattering of Waves: Some Analogies with Quantum Scattering

5. Funding Numbers.
Contract
Program Element No. 0601153N
Project No. 03202
Task No. 340
Accession No. DN255011
Work Unit No. 12212B

6. Author(s).
M. F. Werby

7. Performing Organization Name(s) and Address(es).
Naval Oceanographic and Atmospheric Research Laboratory
Ocean Acoustics and Technology Directorate
Stennis Space Center, MS 39529-5004

8. Performing Organization Report Number.
PR 92:026:221

9. Sponsoring/Monitoring Agency Name(s) and Address(es).
Naval Oceanographic and Atmospheric Research Laboratory
Ocean Acoustics and Technology Directorate
Stennis Space Center, MS 39529-5004

10. Sponsoring/Monitoring Agency Report Number.
PR 92:026:221

11. Supplementary Notes.
Published in American Institute of Physics Conference Proceedings 260, Computational Quantum Physics

12a. Distribution/Availability Statement.
Approved for public release; distribution is unlimited.

12b. Distribution Code.

13. Abstract *(Maximum 200 words).*

The scattering of waves in classical physics and quantum scattering theory have many dissimilarities, but also many things in common. Many of the modern developments in classical wave theory have their origin in quantum scattering despite the later development of quantum physics. Although each field has diverged from the other over time, there are many analogies between the two disciplines and much in one area may enhance the other. In this work an outline is given of some aspects of the classical scattering theory of waves which have some relation with quantum theory. In addition, some numerical techniques are presented that may be of use in both areas.

14. Subject Terms.
Acoustic scattering, shallow water, waveguide propagation

15. Number of Pages.
27

16. Price Code.

17. Security Classification of Report.	18. Security Classification of This Page.	19. Security Classification of Abstract.	20. Limitation of Abstract.
Unclassified	Unclassified	Unclassified	SAR

AMERICAN INSTITUTE OF PHYSICS

AIP CONFERENCE PROCEEDINGS 260

COMPUTATIONAL QUANTUM PHYSICS

NASHVILLE, TN 1991

EDITORS: A. S. UMAR
V. E. OBERACKER
M. R. STRAYER
C. BOTTCHER

The Classical Scattering of Waves: Some Analogies with Quantum Scattering

Michael F. Werby, Theoretical Acoustics and Simulation,
NOARL, Stennis Space Center, MS 39529

Abstract

The scattering of waves in classical physics and quantum scattering theory have many dissimilarities, but also many things in common. Many of the modern developments in classical wave theory have their origin in quantum scattering despite the later development of quantum physics. Although each field has diverged from the other over time, there are many analogies between the two disciplines and much in one area may enhance the other. In this work an outline is given of some aspects of the classical scattering theory of waves which have some relation with quantum theory. In addition, some numerical techniques are presented that may be of use in both areas.

Introduction

As in the field of quantum scattering, one employs the scattering of waves on objects and interfaces to gain knowledge of the scatterer. From targets in the sky to those under the sea, to oil domes under the ground, we use electromagnetic, acoustic, and elastic waves to gain knowledge of what would otherwise elude us. Remarkably, much of the mathematical methodology and some of the physical events, such as resonances in classical scattering occur in quantum scattering and it is likely that the base of knowledge in one area will promote "hybrid vigor" in the other. The purpose of this article is to describe some aspects of the classical scattering of waves from the viewpoint of one familiar with quantum scattering theory and quantum phenomena. The mathematical development to describe scattering from targets that will be emphasized here is based on an exact numerical technique by Peter Waterman, who in a series of beautiful papers,[1-3] outlined the course of treatment that constitutes a unified theory of the classical scattering of waves. The T-matrix or more properly, the extended boundary condition (EBC) method due to Waterman[1-3] is in part an algorithmic method which, in my view, is as powerful in an algorithmic sense as that of Hamilton's principle or the Euler-Lagrange equations. This method (largely overlooked by the classical scattering community) along with numerical or structural improvements has enabled researchers to perform enormously complicated calculations and understand physical phenomena previously not possible.

Along with the formal and numerical procedures outlined here I will discuss some physical phenomena in wave scattering that has some similarities with quantum scattering. In the area of acoustical phenomena such as resonance scattering, Herbert Überall[4–8] has, in my view, been the major contributor, both in introducing techniques and in describing phenomena in the context found in quantum physics. Of particular note is his development of a resonance scattering theory[4] (RST) along lines parallel to that of Briet and Wigner[9] and Kapur and Peierls[10] as well as his realization that resonances excited on elastic targets were mainly due to circumferential waves excited on elastic surfaces that due to phase matching conditions form standing waves at distinct frequencies resulting in the resonance phenomena.[6] Analogies between quantum and classical scattering and propagation are numerous.[11] The treatment of some scattering from submerged particles such as sediment, due to Foldy and Lox, is similar to the adiabatic theory of scattering developed by Foldy. The Born approximation and the related Kirchhoff approximation play an important role in wave scattering, particularly from surfaces. Both a T-matrix and an S-matrix can be defined in wave scattering where the important concept of symmetry, unitarity, and the generalized optical theory play a role.[12, 13] Überall has shown that even Reggie poles[8] find their place in the classical scattering of waves and that one can divide scattering into a superposition of a form of direct scattering (called the background) and resonance scattering just as in quantum scattering. This was done for elastic spheres by Überall in which he employed a rigid scatterer as the background for elastic solids[4] and by Werby using the concept of entrained mass for a shell.[14, 15] The analogy with quantum scattering occurs at low energy where shape elastic scattering adds coherently with resonance scattering due usually to collective motion of the nucleus. Due to space limitations, I will limit my discussions to topics that I have had direct experience with, with it being understood that many more analogies exist between the two areas than presented here. A comprehensive development of the vast area of resonance scattering from elastic targets may be found in a new book by Überall.[7]

Several techniques are available for describing waves that scatter from objects of known constitution and geometry. Many of them are rather specific or have intractable numerical pitfalls. It is therefore desirable to obtain a formulation that allows for general objects, ranges of frequency, and boundary conditions, and that overcomes numerical difficulties commonly encountered in several broad classes of numerical methods. In this paper we briefly describe the Waterman method which proves to be a consistent, unified and manageable numerical approach useful for researchers interested in solving any of a wide class of scattering problems. It is based on the coupling of the exterior and interior solutions of the surface boundary representation of the Helmholtz or elastodynamic equations and yields the EBC method of Waterman.[1–3] The EBC method avoids numerical problems often encountered by other techniques. We present numerous physical examples which are chosen

not only for their intrinsic interest but also because they represent comparatively difficult problems to solve by other means.

We then focus on some of the physical events in wave scattering that have similarities with quantum mechanical events. We first start with a review of the Extended Boundary Condition method for determining the field scattered from a rigid spheroidal object. We next extend this development to include elastic objects. Finally, we describe the time domain solution, partial wave analysis, and additional physical phenomena.

The Extended Boundary Condition Method in Review

The EBC method forms the basis of the equations used here to develop the eigenexpansion and transformation methods that follow. Since emphasis is on the mathematical basis and properties of these two procedures (with the exception of scattering from impenetrable targets, details of EBC equations can be both intricate and extended), we will indicate only the EBC equations for the simplest case, and list the generalizations for more complicated scenarios. The Helmholtz-Poincare' integral representation for a field exterior to a bounded object can be expanded as follows.

$$U(r) = U_i(r) + \int_S \left[U_+(r') \frac{\partial G(r,r')}{\partial n} - G(r,r') \frac{\partial U_+(r')}{\partial n} \right] ds \qquad (1)$$

where r is chosen to be at an exterior point to the object; i.e., r is a member of D, where D is the set of all points exterior to the object, G is an outgoing Green's function, D' is the set of points in the interior of the bounded object, and S is the set of all points on the object surface. The surface of the object is assumed to be piecewise continuous. It is redolent of Gauss' law that when r is in the interior the total wavefield U(r) is zero (extinguished or nulled), hence the terms "extinction theorem" or, "null-field condition." This fact was generally thought inconsequential, but Waterman[1] took specific advantage of this condition to employ a constraint on the exterior solution to eliminate the surface terms U_+ or $\partial U_+(r')/\partial n$, which arise in the exterior solution. Here n is a unit outward normal to the surface. Although Waterman[1] employed the condition algorithmically to eliminate the surface term, he developed a method that also produced a unique solution for all positive frequencies of the exterior problem. This is of considerable importance, because exterior solutions have often suffered from "spurious resonances" at the so-called "irregular values" of incident frequency. These irregular values correspond to the eigenfrequency of a problem related to the interior problem considered here. It has been established that by coupling the interior points in the solution the irregular

values are eliminated. Thus, Waterman's equations actually serve two computational purposes. For completeness we list the interior problem as follows

$$0 = U_i(r'') + \int_S \left[U_+(r') \frac{\partial G(r'',r')}{\partial n} - G(r'',r') \frac{\partial U_+(r')}{\partial n} \right] ds \tag{2}$$

where r'' is an interior point. The above equations constitute the extended boundary condition equations. Since in their present form they are not directly useful, we now reduce them to a form amenable to numerical computation. For convenience of presentation we simplify the problem, to that of an impenetrable object (although solution of the fluid target case is quite similar). Elastic targets submerged in a fluid require far greater mathematical detail, as indicated by Waterman.[3] Let us assume that $\partial U_+(r')/\partial n = 0$ so that we obtain the expressions

$$U(r) = U_i(r) + \int_S \left[U_+(r') \frac{\partial G(r,r')}{\partial n} \right] ds \tag{3}$$

$$0 = U_i(r'') + \int_S \left[U_+(r') \frac{\partial G(r'',r')}{\partial n} \right] ds . \tag{4}$$

To solve these expressions, it is convenient to represent $U_i(r)$, $U_+(r')$ and $G(r,r')$ in some convenient series expansion, which upon truncation would lead to matrix equations that can then be solved using digital computers. The Green's function G is a normal operator, and thus can be represented by the biorthogonal series

$$G(r,r') = i\kappa \sum Re\varphi_i(r_<)\varphi_i(r_>) \tag{5}$$

where $r_<$ and $r_>$ are the greater and lesser of the two points r and r relative to the origin of the object, respectively. The quantity U_i, the incident wavefield, is known. In a manner similar to that of the Hilbert-Schmidt theorem for symmetric kernels, it can be shown that

$$U_i(r) = \sum a_n Re\varphi_n(r) . \tag{6}$$

For incident plane waves, the a's are known. We now have the relation

$$\sum_n a_n \, \mathrm{Re}\varphi_n(r) = i\kappa \sum_n \int \mathrm{Re}\varphi_n(r) U_+(r) \frac{\partial \varphi_i(r')}{\partial n} \, dS \tag{7}$$

where it follows that

$$a_n = i\kappa \int U_+(r) \frac{\partial \varphi_i(r')}{\partial n} \, dS \, . \tag{8}$$

We now wish to represent the above matrix form. This can be achieved by writing $U_+(r')$ in some complete set of known functions so that

$$U_+(r) = \sum_n b_n \, \mathrm{Re}\varphi_n(r) \tag{9}$$

where b_n is the only unknown. This reduces to an expression in which the expansion coefficients b_n are the only quantities to be determined. Note that we are not really concerned with the b_n's as such, but rather are eliminating the unknown surface quantities U_+. We get:

$$a_n = \sum_m b_m \int \mathrm{Re}\varphi_m(r') \frac{\partial \mathrm{Re}\varphi_n(r')}{\partial n} \, dS \tag{10}$$

where Q_{nm} is an element of some known matrix. The $\mathrm{Re}\varphi_m$'s are not the most efficient functions to employ. Our intention is to determine the most efficient expansion functions, i.e., those that would form an orthonormal (ON) basis set on the surface of the bounded object. We then obtain the most effective expansion of U_+ on the object surface.[16, 17] To do so, we premultiply the above equation by the adjoint of Q, namely $Q^\dagger$, where the latter quantity is the complex transpose of Q.

$$Q^\dagger a = iQ^\dagger Q b = i \, Hb \tag{11}$$

where the matrix H can easily be shown to be self-adjoint or Hermitian (where $H^\dagger = H$). The advantage pursuing this course is that we can easily find the eigenvalues and eigenfunctions of H that have known and computationally desirable properties. In particular, the eigenvalues here are real, positive, and increase monotonically, and form an orthonormal set of functions on the surface. The eigenfunctions can be obtained as follows:

$$H\beta_i = \lambda_i\beta_i . \tag{12}$$

Here, the adjoint of β is β^*, so that

$$\beta_i\beta^\dagger_j = \delta_{ij} \tag{13}$$

where δ_{ij} is the Kronecker delta function.

We also have the ordering $\lambda_1 < \lambda_2 < \lambda_3 \ldots$ where the dimension of H is any desired order and relates to the number of surface quantities required in expanding U_+. One can show that the β_i's are an alternate representation of the $\partial\varphi_i(r')/\partial n$'s, with the desired property that they are an orthogonal representation (with another computationally desirable property to be discussed). Thus, we have $b = \sum\alpha_i\beta_i$ so that

$$Q^\dagger a = i\,\Sigma H\alpha_i\beta_i = i\,\Sigma\,\alpha_i\lambda_i\beta_i . \tag{14}$$

Thus $$\alpha_i = -i\beta_i Q^\dagger A/\lambda_i \text{ and } b = -i\,\Sigma\beta_i Q^\dagger A/\lambda_i . \tag{15}$$

We also expand the exterior problem as follows

$$f_j = ik\,\Sigma_i\, b_j\int \mathrm{Re}\,\varphi_j(r')\mathrm{Re}\partial\varphi_i(r)/\partial n\; dS = ik\;\Sigma_i b_j Q_{ij} . \tag{16}$$

The final expression for the scattered field in terms of the incident wave field is thus

$$f = -\Sigma \mathrm{Re}Q\beta_i Q^\dagger A/\lambda_i\beta_i . \tag{17}$$

Although the above expression has proven computationally efficient, it is also possible and sometimes necessary to obtain an alternate T-matrix representation. This may be done by means of the following derived relation:

$$T = -\mathrm{Re}Q\beta(1/\lambda)\;\beta^\dagger Q^\dagger \tag{18}$$

where $\beta\beta^\dagger = \beta^\dagger\beta = I$. The set of eigenvectors β form a unitary matrix and therefore the above expression may be viewed as having been obtained by transforming Q via a unitary matrix obtained from Q times its adjoint. This offers a generalization of this method to one more complicated and that cannot be posed in such a simple form. For the general problem a T-matrix may be written in the form

$$T = -PQ^{-1} \tag{19}$$

with solutions of the form

$$T = -P\beta\;(1/\lambda)\;\beta^\dagger Q^\dagger \tag{20}$$

where $QQ^{\dagger}\beta_i = \lambda_i\beta_i$.

The Elastic T-Matrix

We now consider the case of an elastic object. The equation of motion in a fluid is

$$\nabla^2\vec{U} + k^2\vec{U} = 0 \tag{21}$$

where k is the acoustic wavenumber and U is related to the particle displacement. The equation for motion in an elastic body is

$$\left(k_0^2\right)^{-1}\nabla\nabla\cdot\vec{U} - \left(\kappa_0^2\right)^{-1}\nabla\times\nabla\times\vec{U} + \vec{U} = 0$$

$$k_0^2 = \frac{\rho_0\,\omega^2}{\lambda_0 + 2\mu_0} \text{ and } k_0^2 = \frac{\rho_0\,\omega^2}{\mu_0}. \tag{22}$$

where k_0 and κ_0 are the longitudinal and transverse wavenumbers respectively. The boundary conditions at an interface are:

$$\tilde{n}\cdot\vec{U}_+ = \tilde{n}\cdot\vec{U}_- \quad \tilde{n}\cdot\vec{t}_+ = \tilde{n}\cdot\vec{t}_- \quad \nabla\times\vec{t}_- = 0\,. \tag{23}$$

Where the traction t for the outer (+) and inner (−) surfaces are:

$$\vec{t}_+ = \lambda\tilde{n}\nabla\cdot\vec{U}_+ \quad \vec{t}_- = \lambda\tilde{n}\nabla\cdot\vec{U}_- 2\mu_0\tilde{n}\frac{\partial U_-}{\partial n} + \mu_0\tilde{n}\times(\nabla\times U_-)\,. \tag{24}$$

The Green's Functions G(r, r') and Green's stress triadic Σ(r, r') are:

$$\left(k_0^2\right)^{-1}\nabla\nabla\cdot\bar{G} - \left(\kappa_0^2\right)^{-1}\nabla\times\nabla\times\bar{G} + \bar{G} = -\left(\kappa_0^3\right)^{-1}\bar{I}\delta(r - r') \tag{25}$$

$$\Sigma_+ = \lambda\bar{I}\nabla\cdot\vec{U}_+ \quad \Sigma_- = \lambda\bar{I}\nabla\cdot\bar{G}_- + 2\mu_0\tilde{n}\frac{\partial G_-}{\partial n} + \mu_0\bar{I}\times(\nabla\times\bar{G}_-)\,.$$

The boundary integrals are in the fluid and in the elastic body[18-20]

$$\vec{U}^i + \frac{k^3}{\rho\omega^2}\int_s\int\left[\vec{u}_+ \cdot (\tilde{n} \cdot \bar{\Sigma}) - t_+ \cdot \bar{G}\right]ds = \begin{cases} U \text{ Outside the object} \\ 0 \text{ Inside the object} \end{cases}$$

$$\frac{k_0^3}{\rho_0\omega^2}\int_s\int\left[\vec{u}_- \cdot (\tilde{n} \cdot \bar{\Sigma}_0) - t_- \cdot \bar{G}_0\right]ds = \begin{cases} U \text{ Outside the object} \\ 0 \text{ Inside the object} \end{cases} \qquad (26)$$

We need to solve these equations subject to the boundary conditions at the interfaces and with the appropriate asymptotic boundary conditions. The partial wave expansion functions in the fluid and the elastic body are:[21]

$$\phi_n = \frac{1}{k}\nabla h_n(kr)Y_l^m(\theta,\varphi) \qquad \psi_n^1 = [n(n+1)]^{-1}\nabla \times [rh_n(k_o r)Y_l^m(\theta,\varphi)]$$

$$\psi_n^2 = \frac{1}{\kappa_o}\nabla \times \psi_n^1 \qquad \psi_n^3 = \left(\frac{k_o}{\kappa_o}\right)^{3/2}\frac{1}{k_o}\nabla h_n(k_o r)Y_l^m(\theta,\varphi)\,. \qquad (27)$$

Here the Y's are spherical harmonics and the h's are outgoing spherical Hankel functions. Expand everything into partial wave,

$$\vec{U}^i = \sum_{n=0}^{N} a_n \mathrm{Re}\varphi_n \qquad \vec{U}^f = \sum_{n=0}^{N} f_n\varphi_n \qquad \vec{U}^b = \sum_{n=0}^{N}(\alpha_n \mathrm{Re}\psi_n + \beta_n\psi_n)\,. \qquad (28)$$

The Green's functions are also expanded using biorthogonal expansions for normal operators:

$$\bar{G}(r,r') = i\sum_n \mathrm{Re}\phi_n(r)\phi_n(r') \qquad \bar{G}_o(r,r') = i\sum_n \mathrm{Re}\psi_n(r)\psi_n(r')\,. \qquad (29)$$

Expansion Method to Reduce the BIE to Matrix Form

The T-matrix for the most general case is:[20]

$$T = -\{Q_{rr} - Q_{ro}T^2\}\{R_{ro}T^2 + R_{rr} + iT^2\}^{-1}P_{rr}\{Q_{or} - Q_{oo}T^2\}$$
$$\{R_{ro}T^2 + R_{rr} + iT^2\}^{-1}P_{rr}\}^{-1}\,. \qquad (30)$$

T^2 corresponds to a reflection from the inner face of a shell. For a solid $T^2 = 0$ so that[19]

$$T = -Q_{rr}[R_{rr}]^{-1}P_{rr}\ \{Q_{or}[R_{ro}]^{-1}P_{rr}\}^{-1}. \tag{31}$$

For fluid or sound soft or sound hard objects one has:

$$T = -Q_{rr}\{Q_{or}\}^{-1} \tag{32}$$

where the matrices Q, R, P are as follows:

$$Q_{nn'} = \frac{k^3}{\rho\omega^2}\oint\left[\tilde{n}\cdot\ \mathrm{Re}\psi_{n'}\,\lambda\nabla\cdot\ \phi_n - \tilde{n}\cdot\ t(\mathrm{Re}\psi n_{n'})\tilde{n}\cdot\ \phi_n\right]ds$$

$$R_{nn'} = \frac{k^3}{\rho\omega^2}\oint\left[\mathrm{Re}\psi_{n'}\cdot\ t(\mathrm{Re}\psi_n) - \tilde{n}\cdot\ t(\mathrm{Re}\psi_{n'})\tilde{n}\cdot\ \psi_n\right]ds$$

$$P_{nn'} = \frac{k^3}{\rho\omega^2}\oint\left[\tilde{n}\cdot\ \mathrm{Re}\phi_{n'}\,\tilde{n}\cdot\ t(\mathrm{Re}\psi_n)\right]ds. \tag{33}$$

Unitarity, Symmetry and the S-Matrix

The above, equations are difficult to solve because the matrices are often poorly conditioned. We obviate this problem by a method we refer to as the unitary method which we briefly outline. We know from reciprocity that T is symmetric. Also S is unitary if the target and fluid are not energy absorbing which we assume. We can then write $T = -RP^{-1}$ which is its most general form. Then

$$S = 1 + 2T = 1 - 2RP^{-1} = UP^{-1} \tag{34}$$

where $U = P - 2R$. S now becomes

$$S = S' = P'^{-1}u'. \tag{35}$$

Now write $U = MU$ $P = NP$ where **P** and **U** are unitary and N and M are upper triangular. Then $S = P'^{-1}\,LU'$ where $L = N'^{-1}M'$. But $SS'^{*} = P^{*}LL'^{*}P^{*-1} = 1$ which implies $LL'^{*} = 1$. Which implied L is unitary. That means that L which is a product of two upper triangular matrices is upper triangular. But it has to be lower triangular

too and therefore it has to be diagonal. The diagonal elements have to be real and therefore L is the unit matrix. Thus, $S = UP^{*}$ and that implies $T = (UP^{*} - 1)/2$. This expression is much easier to calculate than expressions dependent upon matrix inversion.[13]

Time Domain Resonance Scattering Theory

The partial wave series that emerges from normal mode theory for separable geometries can be represented in distinct partial waves or modes. It has been shown[4,5] that a representation due to a distinct mode (n) can be written in the form:

$$f_n(\theta) = \frac{2}{ka} e^{2i\xi_n^{(r)}} \left\{ \frac{\left(\frac{1}{2}\right) s\Gamma_n^{(r)}}{\chi - \chi_n^{(r)} + \left(\frac{i}{2}\right)\Gamma_n^{(r)}} + e^{-i\xi_n^{(r)}} \sin \xi_n^{(r)} \right\} \tag{36}$$

where $\chi = ka$, $\chi_n^{(r)}$ is the nth resonance and $\left(\frac{1}{2}\right)\Gamma_n^{(r)}$ the half-width.

Where $e^{2i\xi_n^{(r)}} = -\dfrac{h_n^{(2)'}(x)}{h_n^{(1)'}(x)}$.

Here, the factor $2n + 1$ is absorbed in the expansion coefficient. For the pulse form, a continuous wave (cw) ping is used which corresponds to a very broad frequency range. For each time domain modal component, one has that

$$\mathrm{Re}\int_{-\infty}^{\infty} \frac{\left(\frac{1}{2}\right)\Gamma_n^{(r)}}{\chi - \chi_n^{(r)} + \left(\frac{i}{2}\right)\Gamma_n^{(r)}} e^{-i\chi s}\, d\chi = 2\pi \left(\frac{1}{2}\right)\Gamma_n^{(r)} \sin\left(\chi_n^{(r)} s\right) e^{-\left(\frac{1}{2}\right) s\Gamma_n^{(r)}} \tag{37}$$

That is, at a resonance, the time-domain solution is simply the product of the half-width times a sinusoidal function times an exponential damping factor. From the *time-domain solution* for a nest of resonances (N-m) for a cw ping, one obtains the form

$$p(s) = 2\pi \sum_{n=m}^{N} \left(\frac{1}{2}\right) \Gamma_n^{(r)} \sin\left(\chi_n^{(r)} s\right) e^{-\left(\frac{1}{2}\right) s\Gamma_n^{(r)}} \tag{38}$$

The remaining contributions from backscatter are small due to phase averaging.

It is assumed that calculations are performed in a resonance region for which the resonance widths are fairly constant and the resonance spacing is fairly uniform.[22, 23] This assumption leads to the important expression

$$P(s) = 2\pi\, 2^M \left(\sin\left(\chi_{ave}^{(r)} s\right)\right) \left\{\cos\left(\Delta\chi_{ave}^{(r)} s/2\right)\right\}^M e^{-s\Gamma/2}, \tag{39}$$

where $\chi_{ave}^{(r)} = \frac{1}{2M} \sum_{i=n}^{n+2M} \chi_i^{(r)}$.

Here one sets $n - m = 2M$. It is seen from the above expression:

— The half-width is associated with the decay of the response in the time domain solution: the response decreases exponentially with increasing value of the half-width.

— When the number of adjacent resonances (2M) sensed increases, the return signal becomes more sharply defined and the envelope function (the beats) are more enhanced and clearly defined.

— For larger carrier frequencies, the signal is more oscillatory within the envelope.

Applications of the EBC Method to Various Problems

We first treat scattering from rigid impenetrable objects in a free space. The two simplest cases are for spheroids and for cylinders with hemispherical caps. We focus on spheroids.

Application to Rigid Target

There are two classes of targets for impenetrable problems, i.e., soft and hard scatterers. They do not support body resonances; therefore; we examine acoustic quantities appropriate for nonresonant targets, such as circumferentially diffracted or creeping waves. These arise when scattering end-on from a spheroid in which one observes the return signal at the origin of the signal. The values of the incident wavefield frequency are expressed using the dimensionless quantity kL/2, where L is the object length and k the total wavenumber ($k = 2\pi/L$).

Bistatic angular distributions correspond to measurement of a scattered field at any point in space for some incident wave fixed relative to some source-object orientation. In Figure 1 we examine a rigid spheroid of aspect (length-to-width)

(38)

e averaging.
for which the
uniform.[22, 23]

(39)

me domain
of the half-

the return
s) are more

he envelope.

e. The two
l caps. We

ft and hard
ine acoustic
v diffracted
d in which
he incident
2, where L

ed field at
ırce-object
h-to-width)

ratio of 30:1. Figure 1a and 1b represent scattering from the object along the axis of symmetry (end-on) (a) and 90-degrees relative to the symmetry axis (broadside). The value of kL/2 in Figure 1a and 1b is 200, which implies that the object is about 70 wavelengths long and thus in the intermediate- to high-frequency region where neither low nor high frequency approximations apply. In all figures, frequency is sufficiently high that wave diffraction effects are significant in the forward scattering direction.

There are two competing mechanisms in the backscatter case. One arises from specular scattering (geometric) and the other arises from the creeping waves. The result is a coherent effect in which the two waves add constructively at some point leading to a maximum value when they are in phase and destructively leading to a minimum when they are out of phase. This can be seen in Figure 1 for a spheroid of aspect ratio (c) 4 to 1 (d) 8 to 1 and (e) 16 to 1. The more pronounced dips with increasing aspect ratio is due to the greater grazing angular region for higher aspect ratio targets.

Applications to Elastic Targets

We now examine a phenomenon observed frequently when scattering from elastic objects with smooth boundary conditions surrounded by an acoustic fluid, namely, body resonances. The resonances examined for the elastic solid case originate from the curved-surface equivalents of seismic interface waves of pseudo-Rayleigh or Scholte type, propagating circumferentially to form standing waves on a bounded object or from bending modes when scattering at oblique angles. These types of resonances occur at discrete values of kL/2 and manifest themselves in a characteristic manner. For elongated elastic solids, three distinct resonance types occur. The first kind (at lower frequencies) are due to leaky Rayleigh waves and have been shown to be related to both target geometry and material parameters (notably shear modulus and density). Resonances can, in this case, be best observed by examining the backscattered echo amplitude and phase response plotted as a function of kL/2, often referred to in acoustic scattering literature as a form function. We illustrate this for WC spheroids of aspect ratios of 6, 8, and 10 to 1 end-on incidence in Figure 2a, 2b, and 2c respectively. Here we see two resonances superimposed on the semi-periodic pattern due to Franz waves associated with rigid scattering. If we were to subtract rigid scattering (in partial wave space) from the elastic response then we would be left with the resonance response alone. Note the slight upward shift in kL/2 value with increasing aspect ratio (L/D) which can be explained in terms of standing waves on the surface. In addition to the above wave phenomena, it is also possible to excite "whispering gallery" resonances, which for these examples occur at higher kL/2 values.

In Figure 3 we examine broadside resonances for 2, 3, 4, and 5 to 1 steel spheroids. Here we can excite three phenomena. At the lowest value we can see a spike

representing a bending resonance (Werby and Gaunaurd[24]) discussed below. The second lowest spike corresponds to the lower order Rayleigh resonance seen end-on, corresponding to a standing wave, circumnavigating the largest meridian of the spheroid. We also see weak Franz waves similar to those excited on a cylinder, and then we see the lowest order Rayleigh and Whispering Gallery resonances corresponding to circumferential waves around the smallest meridian. The third kind we wish to illustrate has to do with bending modes or flexural resonances. For unsupported spheroids, a plane incident wave at 45 degrees relative to the axis of symmetry can excite these modes illustrated in Figure 4a through 4d for aspect ratios of 2:1 through 5:1. It can be shown that the lowest mode corresponds to 2, and thereafter 3, 4, etc. The interesting thing about these resonances is they can be predicted by exact bar theories and coincide nicely with results here. Of particular interest is the effect that with increasing aspect ratio, the onset of resonances occur at lower kL/2 values, the opposite observed in Rayleigh resonances.

Finally, we examine scattering from a thin elastic aluminum spheroidal shell. Figure 5a, 5b, and 5c illustrates scattering end-on, at 45 degrees relative to the axis of symmetry and broadside. As noted earlier by Werby and Gaunaurd,[25] one can only excite resonances due to modal vibrations corresponding to standing waves about the largest meridian (end-on) and modal vibrations corresponding to standing, to modal vibrations about the shortest meridian (broadside). Further, it is possible to excite bending modes at oblique angles. In fact, the lowest nulls in Figure 5b and 5c correspond to the lowest (n = 2) bending mode. Evidence of bending modes can be seen at higher frequencies as slight nulls in the two figures and are the thin shell analogues of the elastic solid case. Here they appear as nulls instead of spikes due to a change of phase of 180 degrees in acoustic background (from rigid to soft).

Resonance Phenomena, Time Domain, and Partial Waves

Flexural waves do not yield resonances from fluid-loaded shells until the phase velocity of the flexural wave is about equal to the speed of sound in the ambient fluid.[22, 23, 26] The value in frequency for which this happens is referred to as the coincidence frequency; however, some subsonic fluid-borne waves produce sharp[19,20] resonances below coincidence frequency. These waves are referred to as pseudo-Stoneley waves and the related resonances as pseudo-Stoneley resonances.[22, 23, 27] The pseudo-Stoneley resonances are well defined in partial wave space; they usually correspond to only one partial wave mode number and a very narrow half-width with a dispersive phase velocity, which approaches the speed of sound in the fluid with increasing frequency. The pseudo-Stoneley resonances diminish in significance at the point where the flexural resonances begin to dominate. It can be determined that a phase change occurs in the pressure field in the transition region from subsonic to supersonic. This change accounts for the envelope of the resonance curve at

coincidence frequency where the waves are in phase until coincidence, and are out of phase afterwards. Our interest here is in examining the time-domain response, since one expects the conditions previously described to be partially met over a broad frequency range, and thus to yield a strong coherent response with a carrier frequency in the neighborhood of the frequency at coincidence. Accordingly, the case of cw pings for two examples—for which coincidence resonances are expected to arise—is examined. This is certainly suggested by the strong responses in Figure 6b at the ka value 45, for WC. Further, in this analysis, the Mindlin-Timoshenko[28] thick plate theory is used to determine the value for which the flexural phase velocity will equal the ambient speed of sound in water. The phase and group velocities are determined from flat plate theory, which proves to be quite reliable in predicting the phase velocity for the curved surfaces of the spheres at the coincidence frequency.

The time-domain calculations are now examined. The example is a WC shell of 1% thickness. In this case, a well-defined envelope (illustrated in Fig. 6a) with pronounced oscillations within the envelope, is consistent with Eq. 39. The enhancement due to the factor 2^M is obvious here for the WC case. The group velocity can be obtained from the peak-to-peak distance of the adjacent envelopes. The result leads to a value of 2.33 km/sec. Both flexural and pseudo-Stoneley resonances compete in this region. A mixture of pseudo-Stoneley waves, as well as flexural waves, must be leaking into the fluid. For flexural waves, the group velocity is 2.65 km/sec at coincidence frequency with a range between 2.49 and 2.78 km/sec over the ka range of 30–60, where the strong flexurals are significant. In that range the phase velocity varies from 1.37 to 1.58 km/sec. The value of the extracted group velocity does not agree well with the flexural group velocity; the discrepancy is 12%. This variation suggests that the flexural resonances are of little importance for the time sequence presented here. The group velocity of the pseudo-Stoneley waves for this case has been determined[27] to be 2.65 km/sec based on plate theory. The phase velocity is in the range from 88% to 98% of the speed of sound in the fluid. This value of group velocity is within 3% of the extracted value from the time-domain solution. Moreover, the pseudo-Stoneley resonances have very narrow widths, while the flexural resonances are quite large. The conditions in a previous section would indicate that the flexural resonances would rapidly dampen due to the large half-widths, while the pseudo-Stoneley resonances would attenuate slowly in time. Thus, based on the similarity of the extracted group velocity and that of the pseudo-Stoneley wave and the conditions in the previous section on level widths, one may conclude that the time-domain calculations in Figure 6a represent pseudo-Stoneley resonances.

It is of some interest to discuss resonance scattering from elastic targets because of the close analogy to low energy nuclear resonance scattering. It was mentioned earlier that one can describe the resonance return signal as a function of the nondimensionalized frequency ka (excitation function for the nuclear case) as a

resonance term and a background term (shape elastic scattering in low energy nuclear scattering). To show this, Figure 7a illustrates the total backscattered response from a steel spheroid (length to width of 3 to 1) end-on incidence. Figure 7b illustrates the resonance return signal obtained by subtracting the rigid background. The resonances are labeled according to the fundamental group ([n, 1] with n = 2, 3, . . .) and the higher-order group ([n, l] with $l = 2, 3, \ldots$ and $n = 0, 1, 2, \ldots$) in analogy to the ground state and excited states of a nucleus. The series [n, 1] is referred to as the Rayleigh series R_1, while the higher order series has been labeled as a Whispering Gallery resonance because of the presumed analogy with the phenomenon at St. Paul's Cathedral in London. To illustrate that these resonances form standing waves on the surface of the object and to suggest the origin of the labeling, we plot the residual bistatic angular distribution (illustrated in Figure 8) as a function of the angle in a plane of the object. It is clear that we observe dipole, quadruple, etc. terms according to the "N" designation for both classes of waves consistent with the Überall notion of this class or resonances. Although is has been commonly assumed that Überall's notions for elastic solid spheres are accepted, these calculations form the basis for establishing that the notions are also valid for a spheroid.[29]

The theory of partial wave analysis often used in nuclear physics has found a useful place in resonance analysis of elastic scattering. Large resonance returns have been noted in scattering from elastic shells. In Figure 9a the analysis used[30] to resolve the matter of the origin of these resonances is illustrated. It has been determined that the sharp spikes correspond to waterborne waves, referred to as pseudo-Stoneley waves, superimposed on broad overlapping flexure resonances. Figure 9b illustrates this effect by examining the contributing partial waves for a fixed frequency. N = 32 corresponds to the sharp waterborne wave and n = 28 corresponds to the broad flexural resonance. N = 6 relates to a fast symmetric mode.

Finally we illustrate a "level diagram" in Figure 10 for WC spheroids for aspect ratios ranging from 1 to 4 in steps of 0.25. We see that the Rayleigh resonances gradually shift upward with increasing ratio while the Whispering Gallery resonances shift up more rapidly for fixed index N. Eventually, the Whispering Gallery resonances shift upward to the extent that they cross over[31] the Rayleigh resonances. We have referred to this as "level crossing" in analogy with a similar event for prolate nuclei.[32]

Acknowledgments

I wish to thank NOARL management and the Office of Naval Research for support of this work. I am indebted to M. Strayer, C. Bottcher and S. Umar for the invitation to their stimulating conference on Quantum Scattering. Shortly after the conference and during the time I was preparing this paper, my father, Michael Moises Werby, passed away. I wish to dedicate this paper in honor of him and the dear memories that will linger on. NOARL contribution number JA 221:010:92.

References

1. P. C. Waterman, J. Acoust. Soc. Am. **45**, 1417 (1969).
2. P. C. Waterman, *Proc. IEEE*, 53(3), 802 (1965).
3. P. C. Waterman, J. Acoust. Soc. Am. **63**(6), 1320 (1977).
4. H. Überall, in *Proceedings of the IUTAM Symposium: Modern Problems in Elastic Wave Propagation*, edited by J. Miklowitz and J. D. Auchenbach, (Wiley Interscience, New York, 1978), pp. 239–263.
5. L. Flax, G. C. Gaunaurd, and H. Überall, in *Physical Acoustics*, edited by W. P. Mason and R. N. Thurston, (Academic Press, 1981), vol. 15, ch. 3, pp. 191–294.
6. H. Überall, L. R. Dragonette, and L. Flax, J. Acoust. Soc. Am. **61**, pp. 711–715 (1977).
7. H. Überall, Editor, *Acoustical Resonance Scattering*, (Gordon and Breach, New York, in press).
8. H. Überall, et al., Appl. Mech. Rev. **43**(10) (1990).
9. G. B. Briet and E. P. Wigner, Phys. Rev. **49**, 519 (1936).
10. P. L. Kapur and Peierls, Proc. Roy. Soc., London, A166, 277 (1938).
11. J. B. Keller, "Progress and Prospects in the Theory of Linear Wave Propagation", SIAM SEREV **21**(2), 229–245 (1979).
12. P. C. Waterman, Phys. Rev. **D 3**, 825–839 (1971).
13. M. F. Werby and L. R. Green, J. Acoust. Soc. Am. **74**(2), 625 (1983).
14. M. F. Werby, Acoustic Lett. **15**, (4), 65–69 (1991).
15. M. F. Werby, J. Acoust. Soc. Am., Dec. (1991).
16. M. F. Werby and S. Chin-Bing, Int. J. Comp. Math. Appls. **11**(7/8), 717 (1985).
17. M. F. Werby, G. Tango, and L. H. Green, in *Computational Acoustics: Algorithms and Applications*, edited by D. Lee, R. L. Sternberg, M. H. Schultz (Elsevier Science Publishers B. V., North Holland, 1988), vol. 2, pp. 257–278.
18. Y.-H. Pao and V. Varatharajulu, J. Acoust. Soc. Am. **60**(7), 1361 (1976).
19. A. Bostrom, J. Acoust. Soc. Am. **67**(2), 390 (1980).
20. B. A. Peterson, V. V. Varadan, and V. K. Varadan, J. Acoust. Soc. Am. **74**(5), 1051 (1983).
21. M. F. Werby and G. J. Tango, Eng. Analysis, **5**(1), 12–20 (1988).
22. M. F. Werby and H. B. Ali, in *Computational Acoustics* edited by D. Lee, Cakmak, R. Vichnevetsky (Elsevier Science Publishers B. V., North Holland, 1990), vol. 2, pp. 133–158.
23. M. F. Werby, Acoustic Lett. **15**(3) 39–42 (1991).
24. M. F. Werby and G. C. Gaunaurd, J. Acoust. Soc. Am. **85**, 2365–2371 (1989).
25. M. F. Werby and G. C. Gaunaurd, J. Acoust. Soc. Am. **82**, 1369 (1987).
26. M. F. Werby and G. C. Gaunaurd, SPIE, Automatic Object Recognition, vol. 1471, 2–17 (1991).

27. M. Talmant, H. Überall, R. D. Miller, M. F. Werby, and J. W. Dickey, J. Acoust. Soc. Am. **86**, 278–289 (1989).

28. D. Ross, *Mechanics of Underwater Noise*, New York: Pergamon Press (1976); S. P. Timoshenko, Philos. Mag. **43**:125–131 (1922).

29. M. F. Werby, et al., J. Acoust. Soc. Am. **84**, 1425 (1988).

30. G. C. Gaunaurd and M. F. Werby, J. Acoust. Soc. Am. **90**, 2539–2550 (1991).

31. M. F. Werby, et al., J. Acoust. Soc. Am. **88**, 2822–2929 (1990).

32. S. G. Nilsson, K. Dan. Vidensk. Selsk. Mat. Fys. Medd. **29**, No. 16 (1955).

t. Acoust.

:s (1976);

50 (1991).

16 (1955).

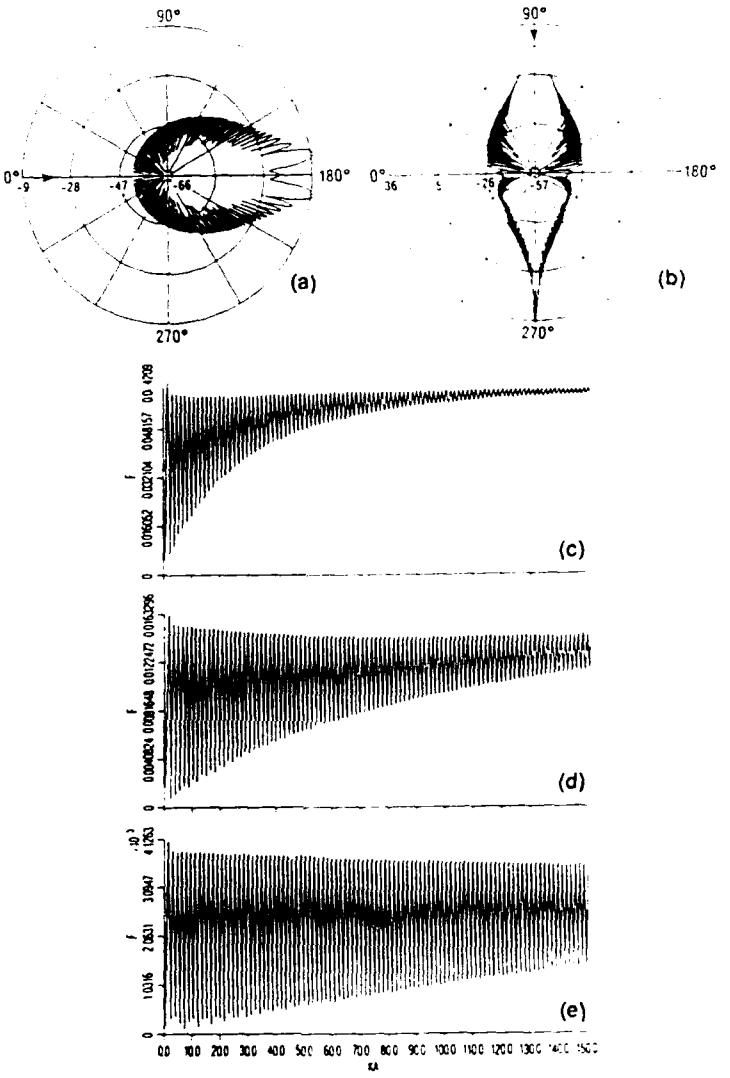

Figure 1. (a) Bistatic scattering from a 30-to-1 aspect ratio rigid spheroid end on; (b) broadside incidence for kL/2 = 200; backscatter from spheroid of aspect ratio of; (c) 4 to 1; (d) 8 to 1; and (e) 16 to 1 for kL/2 = 0 to 150.

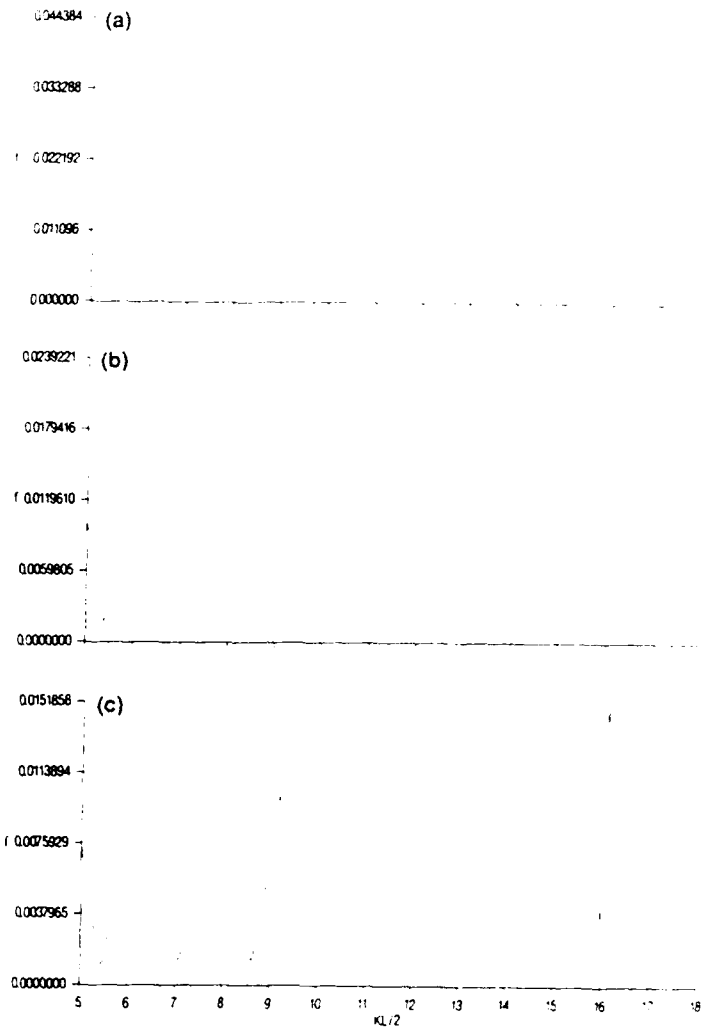

Figure 2. Backscatter from solid WC spheroid end on incidence for aspect ratio of (a) 6 to 1; (b) 8 to 1; and (c) 10 to 1 for kL/2 = 5 to 18.

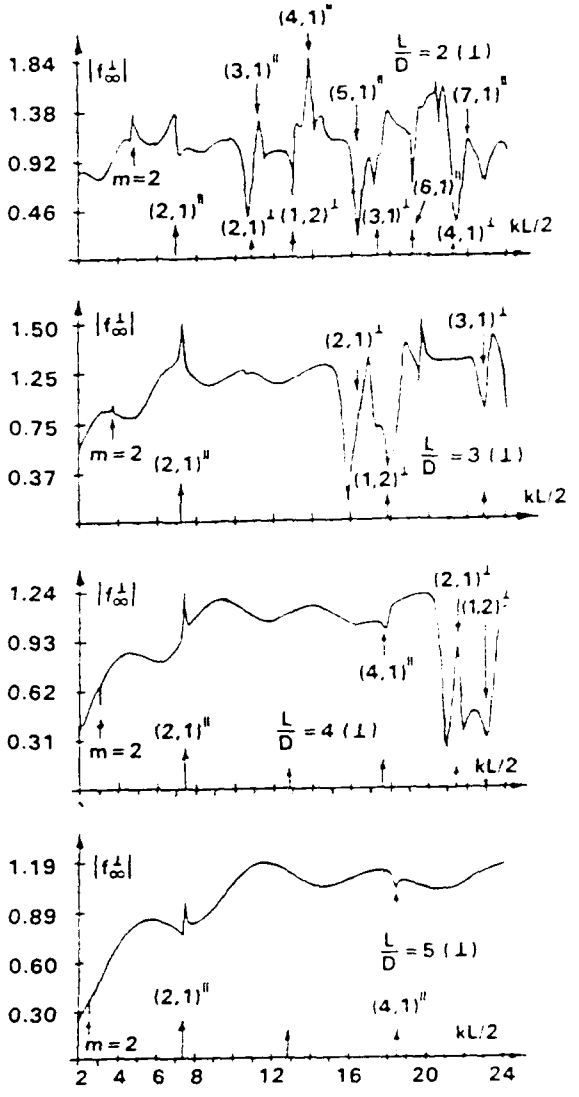

Figure 3. Backscatter from solid steel spheroid broadside incidence for aspect ratio of (a) 2 to 1; (b) 3 to 1; (c) 4 to 1; and (d) 5 to 1 for kL/2 = 2 to 24.

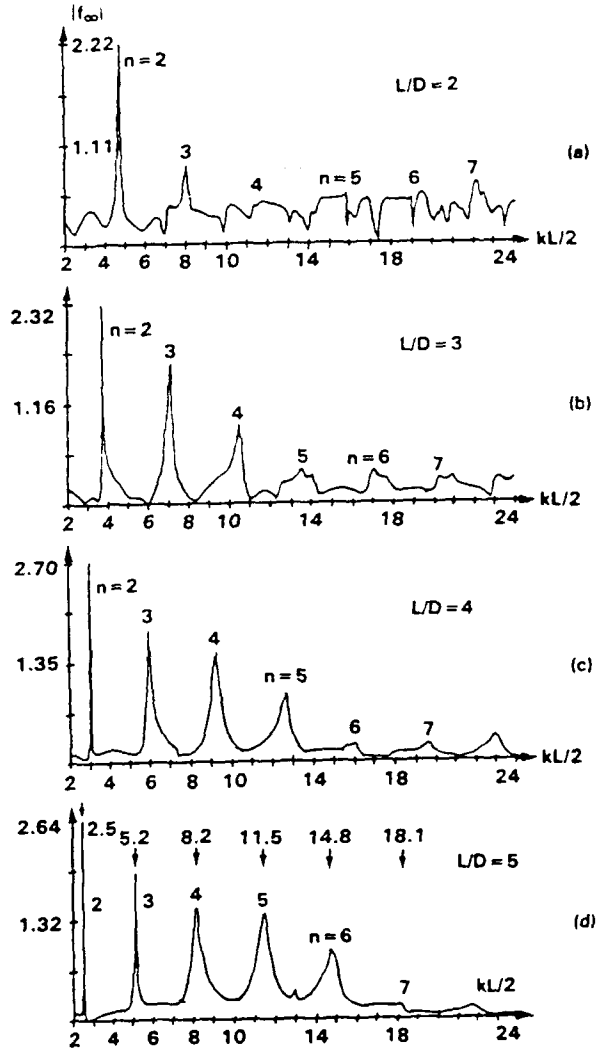

Figure 4. Backscatter from solid steel spheroid at incidence of 45° relative to axis of symmetry for aspect ratio of (a) 2 to 1; (b) 3 to 1; (c) 4 to 1; and (d) 5 to 1 for kL/2 = 2 to 24.

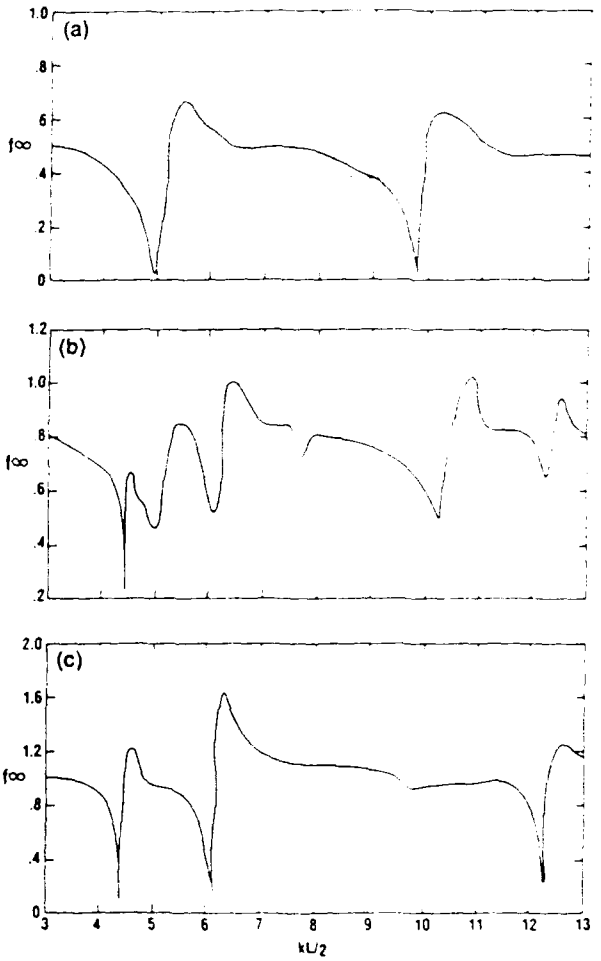

Figure 5. Backscatter from steel spheroidal shell of aspect ratio of 1.5 to 1 (a) backscatter; (b) 45° relative to the axis of symmetry; and (c) broadside.

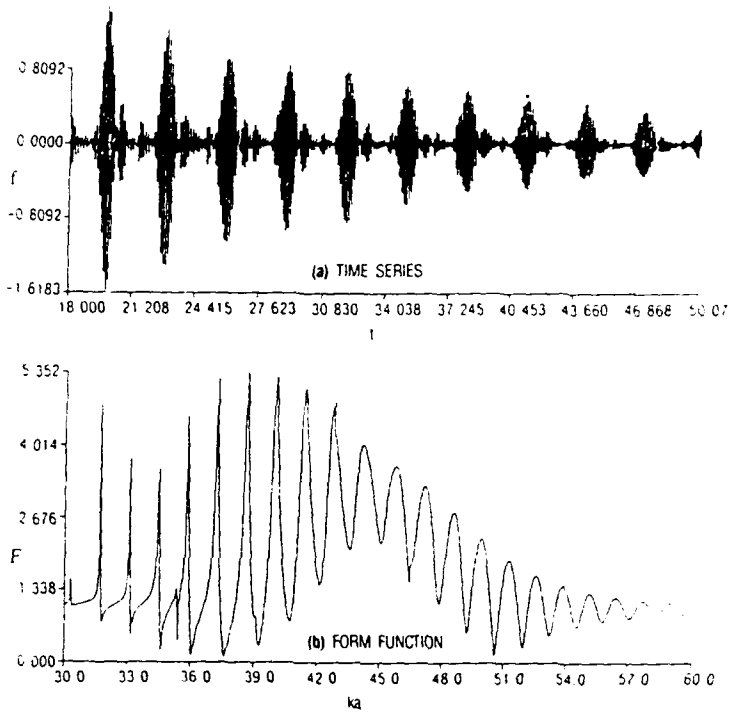

Figure 6. (a) Time domain scattering from a 2.5% thick WC shell from 18 microseconds to 50.07 and (b) backscattered echoes from a 2.5% WC shell from ka = 30–60.

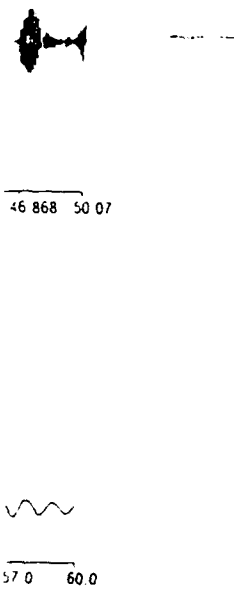

WC shell from
a 2.5% WC shell

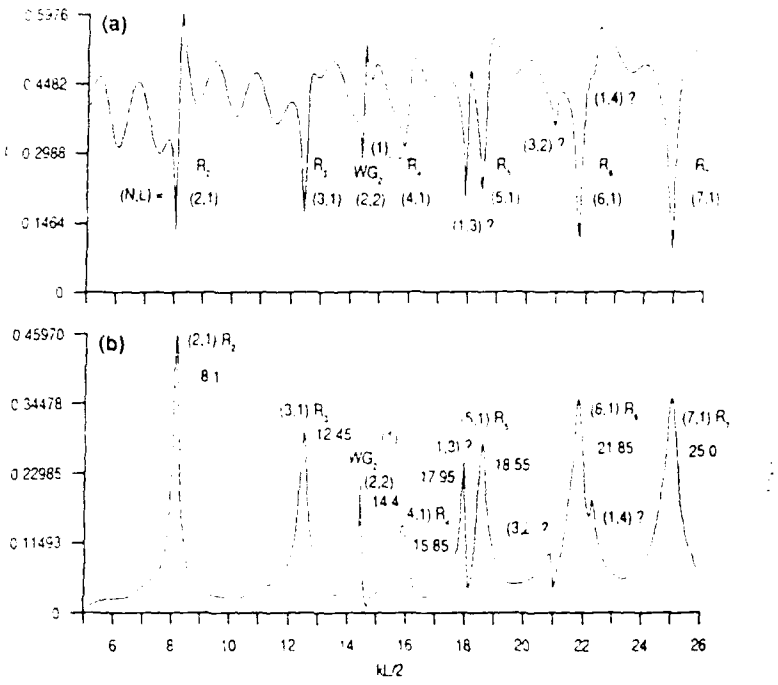

Figure 7. (a) Resonance scattering from a steel spheroid from kL/2 = 0–26 and (b) resonance scattering from a steel spheroid from kL/2 = 0–26 minus a rigid background.

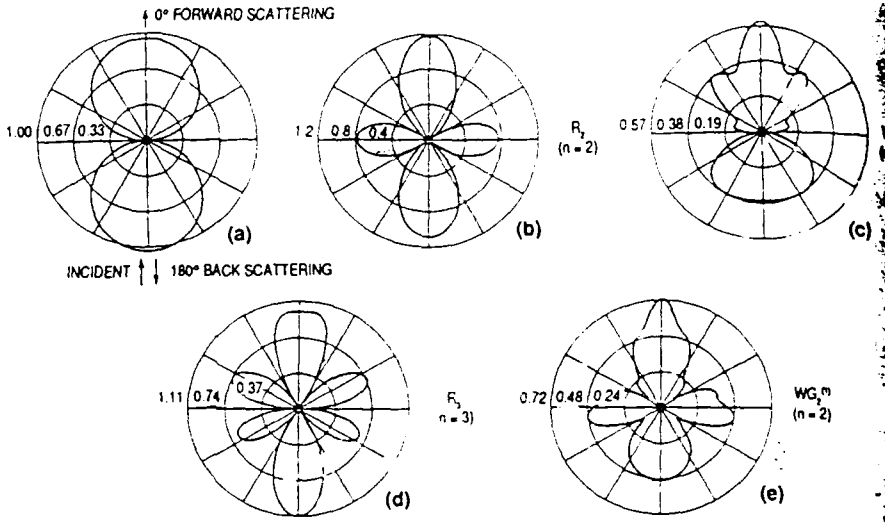

Figure 8. Bistatic scattering of the residual echoes from resonances listed in Figure 7b.

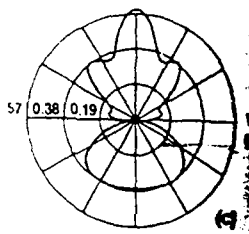

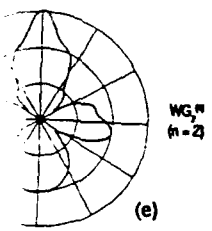

ances listed in Figure 7b.

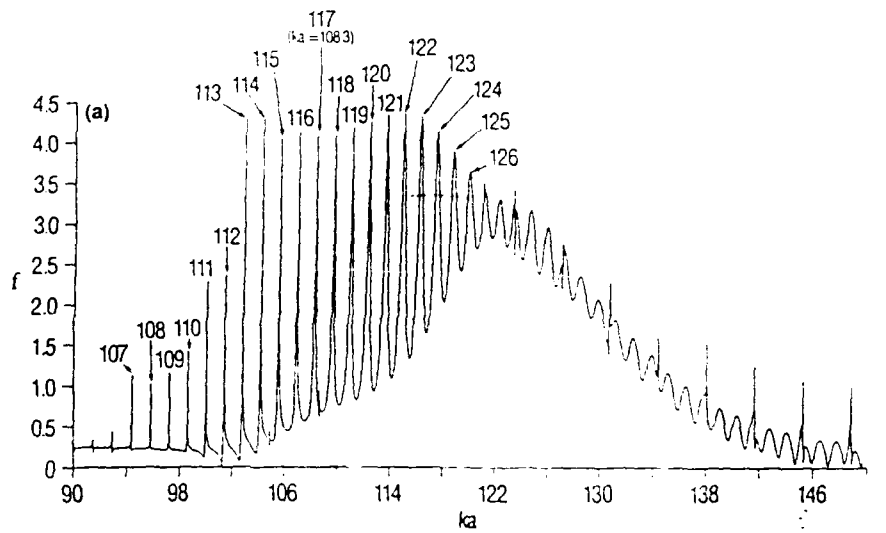

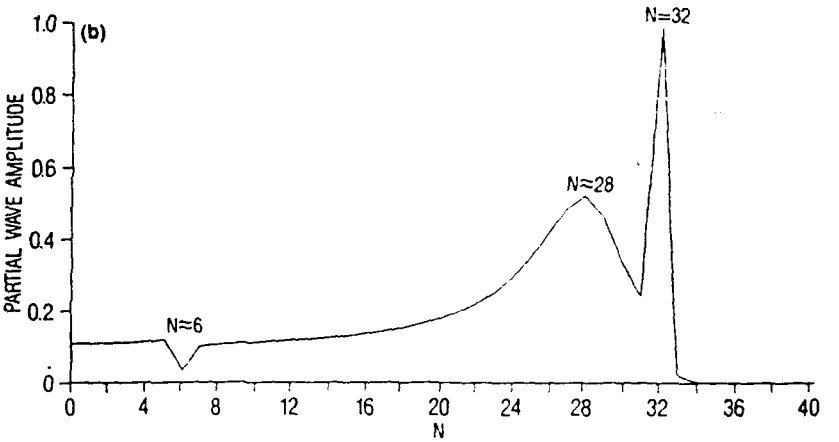

Figure 9. (a) The residual backscattered echo from a 1% thick steel shell and (b) example of a partial wave analysis for the coincidence frequency case for a 2.5% thick WC shell for ka = 33.

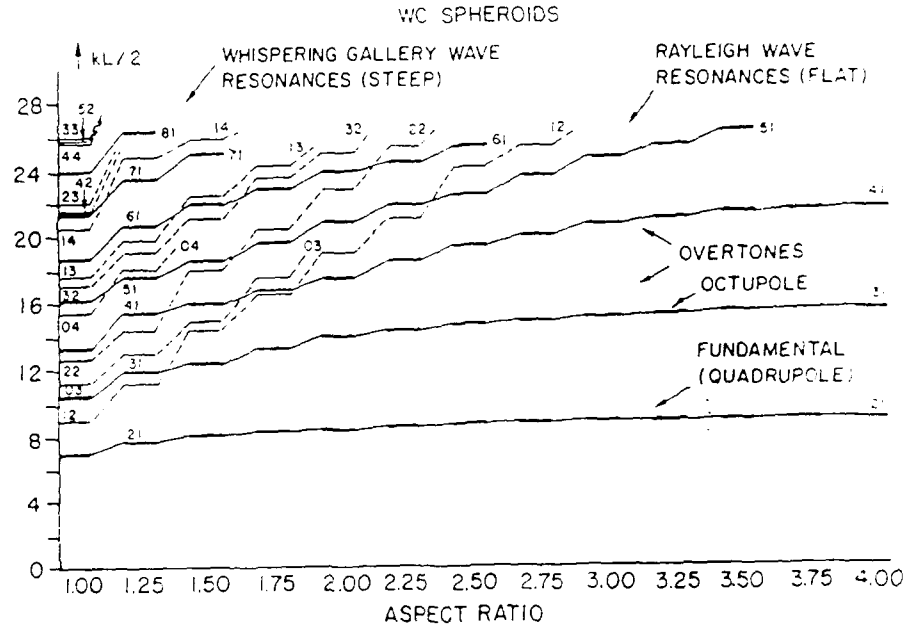

Figure 10. Spectroscopic diagram as a function of aspect ratio of WC spheroidal shells for Rayleigh and Whispering Gallery resonances.